Supporting information for:

Investigation of structure-properties relationship in a novel family of halogenoantimonates(III) and halogenobismuthates(III) with morpholinium cation: $[NH_2(C_2H_4)_2O]MX_4$. Crystal structure, phase transitions and dynamics of molecules.

M. Owczarek[a,b*], R. Jakubas[a], A. Pietraszko[c], W. Medycki[d], J. Baran[c]

[a]*Faculty of Chemistry, University of Wrocław, F. Joliot-Curie 14, 50-383 Wrocław, Poland*
[b]*Laboratory of Neutron Physics, Joint Institute for Nuclear Research, 141-980 Dubna, Russia*
[c]*Institute of Low Temperature and Structural Research of the PAS, 2 Okólna, Wrocław, Poland*
[d]*Institute of Molecular Physics, PAS , M. Smoluchowskiego 17, 60-179 Poznań, Poland*

1 Thermal properties of [*morph*]$SbCl_4$ and [*morph*]$SbBr_4$

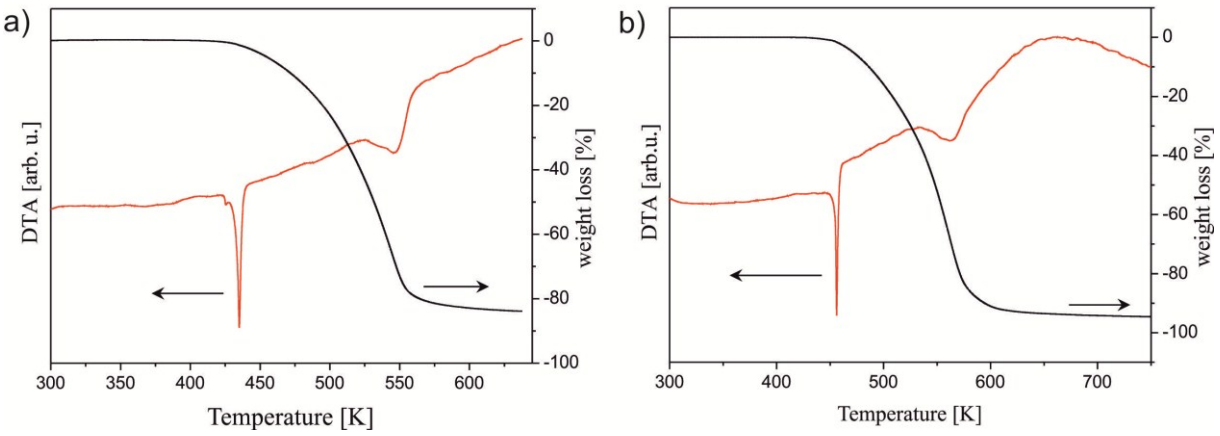

Figure S1. Simultaneous thermogravimetric and differential thermal analyses scan (ramp rate: 2 K/min) for [*morph*]$SbCl_4$ (a) and [*morph*]$SbBr_4$ (b).

2 Crystal structure of [*morph*]$SbCl_4$ and [*morph*]$SbBr_4$

Table S1. Selected bond lengths (Å) and angles (°) for MX_6^{3-} moieties (M = Sb, X = Cl, Br) of [*morph*]$SbCl_4$ and [*morph*]$SbBr_4$ at 100 K.

$[NH_2(C_2H_4)_2O]SbCl_4$			
Sb(1)-Cl(4)	2.3798(5)	Cl(2)-Sb(1)-Cl(3)	172.520(8)
Sb(1)-Cl(1)	2.4031(6)	Cl(4)-Sb(1)-Cl(3)^{i}	81.56(2)
Sb(1)-Cl(2)	2.4897(7)	Cl(1)-Sb(1)-Cl(3)^{i}	168.328(9)
Sb(1)-Cl(3)	2.8456(8)	Cl(2)-Sb(1)-Cl(3)^{i}	83.58(2)
Sb(1)-Cl(3)^{i}	3.1240(7)	Cl(3)-Sb(1)-Cl(3)^{i}	103.89(2)
Sb(1)-Cl(2)^{ii}	3.2832(7)	Cl(4)-Sb(1)-Cl(2)^{ii}	163.029(9)
Cl(4)-Sb(1)-Cl(1)	92.05(2)	Cl(1)-Sb(1)-Cl(2)^{ii}	82.79(2)
Cl(4)-Sb(1)-Cl(2)	92.79(2)	Cl(2)-Sb(1)-Cl(2)^{ii}	103.03(2)
Cl(1)-Sb(1)-Cl(2)	87.016(19)	Cl(3)-Sb(1)-Cl(2)^{ii}	75.56(2)

Cl(4)-Sb(1)-Cl(3)	87.96(2)	Cl(3)^{i}-Sb(1)-Cl(2)^{ii}	106.03(2)
Cl(1)-Sb(1)-Cl(3)	85.519(18)		

$[NH_2(C_2H_4)_2O]SbBr_4$

Sb(1)-Br(4)	2.5448(7)	Br(2)-Sb(1)-Br(3)	172.803(15)
Sb(1)-Br(1)	2.5774(8)	Br(4)-Sb(1)-Br(3)^{i}	82.96(3)
Sb(1)-Br(2)	2.6556(10)	Br(1)-Sb(1)-Br(3)^{i}	169.244(16)
Sb(1)-Br(3)	3.0113(12)	Br(2)-Sb(1)-Br(3)^{i}	84.00(3)
Sb(1)-Br(3)^{i}	3.2042(9)	Br(3)-Sb(1)-Br(3)^{i}	102.39(3)
Sb(1)-Br(2)^{ii}	3.3266(10)	Br(4)-Sb(1)-Br(2)^{ii}	165.639(16)
Br(4)-Sb(1)-Br(1)	92.42(3)	Br(1)-Sb(1)-Br(2)^{ii}	85.07(3)
Br(4)-Sb(1)-Br(2)	95.10(3)	Br(2)-Sb(1)-Br(2)^{ii}	98.87(3)
Br(1)-Sb(1)-Br(2)	86.76(3)	Br(3)-Sb(1)-Br(2)^{ii}	76.74(3)
Br(4)-Sb(1)-Br(3)	89.02(3)	Br(3)^{i}-Sb(1)-Br(2)^{ii}	101.76(3)
Br(1)-Sb(1)-Br(3)	87.18(2)		

Symmetry codes: (*i*) -*x*+3/2, *y*-1/2, *z*; (*ii*) -*x*+3/2, *y*+1/2, *z*.

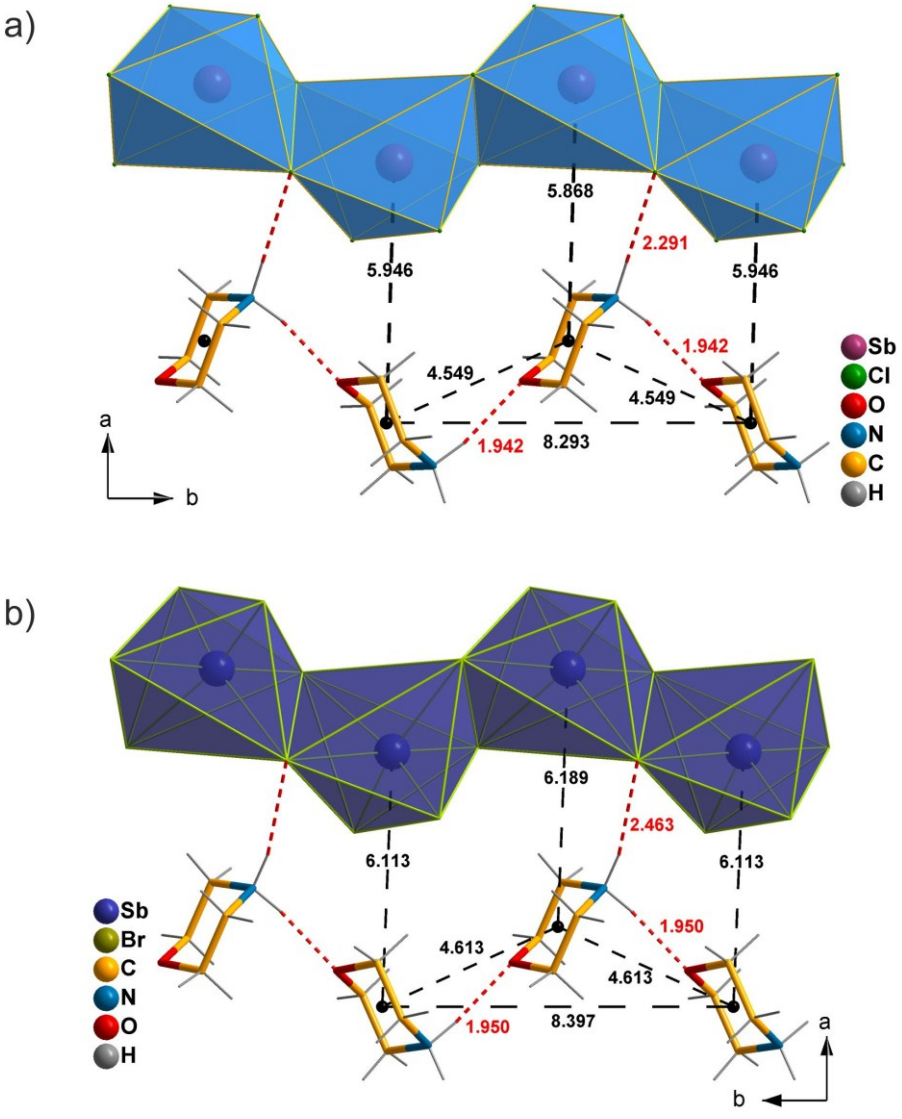

Figure S2. Selected structural parameters of [*morph*]$SbCl_4$ (a) and [*morph*]$SbBr_4$ (b).

3 Crystal structure of [*morph*]$BiBr_4$

Table S2. Selected bond lengths (Å) and angles (°) for $[BiBr_6]^{3-}$ moieties of [*morph*]$BiBr_4$ at 346, 300 and 210 K.

$[NH_2(C_2H_4)_2O]BiBr_4$			
346 K - phase I			
Bi(1)-Br(2)	2.6823(6)	Br(4)-Bi(1)-Br(3)	178.229(13)
Bi(1)-Br(1)	2.7117(6)	Br(2)-Bi(1)-Br(3)^{i}	90.81(2)
Bi(1)-Br(4)	2.8816(10)	Br(1)-Bi(1)-Br(3)^{i}	172.908(12)
Bi(1)-Br(3)	2.9187(10)	Br(4)-Bi(1)-Br(3)^{i}	86.278(18)
Bi(1)-Br(3)^{i}	3.0961(6)	Br(3)-Bi(1)-Br(3)^{i}	93.584(18)
Bi(1)-Br(4)^{ii}	3.1653(6)	Br(2)-Bi(1)-Br(4)^{ii}	172.403(12)
Br(3)-Bi(1)^{ii}	3.0961(6)	Br(1)-Bi(1)-Br(4)^{ii}	91.77(2)
Br(4)-Bi(1)^{i}	3.1653(6)	Br(4)-Bi(1)-Br(4)^{ii}	93.841(18)
Br(2)-Bi(1)-Br(1)	92.49(2)	Br(3)-Bi(1)-Br(4)^{ii}	84.388(19)
Br(2)-Bi(1)-Br(4)	92.64(2)	Br(3)^{i}-Bi(1)-Br(4)^{ii}	85.67(2)
Br(1)-Bi(1)-Br(4)	87.30(2)	Bi(1)-Br(3)-Bi(1)^{ii}	95.033(19)
Br(2)-Bi(1)-Br(3)	89.13(2)	Bi(1)-Br(4)-Bi(1)^{i}	94.298(18)
Br(1)-Bi(1)-Br(3)	92.74(2)		
300 K - phase II			
Bi(1)-Br(2)	2.6567(4)	Br(4)-Bi(1)-Br(3)	175.841(7)
Bi(1)-Br(1)	2.6628(4)	Br(2)-Bi(1)-Br(3)^{i}	85.250(18)
Bi(1)-Br(4)	2.8006(10)	Br(1)-Bi(1)-Br(3)^{i}	170.534(7)
Bi(1)-Br(3)	3.0015(10)	Br(4)-Bi(1)-Br(3)^{i}	83.337(16)
Bi(1)-Br(3)^{i}	3.1474(5)	Br(3)-Bi(1)-Br(3)^{i}	99.643(16)
Bi(1)-Br(4)^{ii}	3.1642(5)	Br(2)-Bi(1)-Br(4)^{ii}	167.502(8)
Br(4)-Bi(1)^{i}	3.1642(5)	Br(1)-Bi(1)-Br(4)^{ii}	90.124(18)
Br(3)-Bi(1)^{ii}	3.1474(5)	Br(4)-Bi(1)-Br(4)^{ii}	97.011(16)
Br(2)-Bi(1)-Br(1)	92.518(17)	Br(3)-Bi(1)-Br(4)^{ii}	79.942(17)
Br(2)-Bi(1)-Br(4)	95.30(2)	Br(3)^{i}-Bi(1)-Br(4)^{ii}	94.030(18)
Br(1)-Bi(1)-Br(4)	87.720(18)	Bi(1)-Br(4)-Bi(1)^{i}	99.973(17)
Br(2)-Bi(1)-Br(3)	87.87(2)	Bi(1)-Br(3)-Bi(1)^{ii}	96.108(16)
Br(1)-Bi(1)-Br(3)	89.449(18)		
210 K - phase III			
Bi(1)-Br(5)	2.6549(8)	Br(5)-Bi(1)-Br(3)	166.224(18)
Bi(1)-Br(6)	2.6937(8)	Br(6)-Bi(1)-Br(3)	88.44(2)
Bi(1)-Br(2)^{iii}	2.8313(8)	Br(2)^{iii}-Bi(1)-Br(3)	100.31(2)
Bi(1)-Br(1)	2.9510(8)	Br(1)-Bi(1)-Br(3)	79.28(2)
Bi(1)-Br(4)^{iii}	3.0905(8)	Br(4)^{iii}-Bi(1)-Br(3)	94.36(2)
Bi(1)-Br(3)	3.1471(8)	Br(7)-Bi(2)-Br(8)	92.84(2)
Bi(2)-Br(7)	2.6448(8)	Br(7)-Bi(2)-Br(3)	87.77(2)
Bi(2)-Br(8)	2.6536(8)	Br(8)-Bi(2)-Br(3)	96.11(2)
Bi(2)-Br(3)	2.7554(8)	Br(7)-Bi(2)-Br(4)	88.77(2)
Bi(2)-Br(4)	3.0565(8)	Br(8)-Bi(2)-Br(4)	89.76(2)
Bi(2)-Br(2)	3.1574(8)	Br(3)-Bi(2)-Br(4)	173.33(2)
Bi(2)-Br(1)	3.1812(8)	Br(7)-Bi(2)-Br(2)	91.51(2)
Br(2)-Bi(1)^{iv}	2.8313(8)	Br(8)-Bi(2)-Br(2)	168.402(18)
Br(4)-Bi(1)^{iv}	3.0905(8)	Br(3)-Bi(2)-Br(2)	94.80(2)
Br(5)-Bi(1)-Br(6)	92.41(2)	Br(4)-Bi(2)-Br(2)	79.59(2)
Br(5)-Bi(1)-Br(2)^{iii}	93.46(2)	Br(7)-Bi(2)-Br(1)	168.474(19)
Br(6)-Bi(1)-Br(2)^{iii}	88.20(2)	Br(8)-Bi(2)-Br(1)	83.85(2)
Br(5)-Bi(1)-Br(1)	86.97(2)	Br(3)-Bi(2)-Br(1)	81.63(2)
Br(6)-Bi(1)-Br(1)	89.72(2)	Br(4)-Bi(2)-Br(1)	102.23(2)
Br(2)^{iii}-Bi(1)-Br(1)	177.89(2)	Br(2)-Bi(2)-Br(1)	93.86(2)

Br(5)-Bi(1)-Br(4)^{iii}	86.57(2)	Bi(1)-Br(1)-Bi(2)	96.66(2)
Br(6)-Bi(1)-Br(4)^{iii}	172.337(19)	Bi(1)^{iv}-Br(2)-Bi(2)	99.43(2)
Br(2)^{iii}-Bi(1)-Br(4)^{iii}	84.28(2)	Bi(2)-Br(3)-Bi(1)	101.67(2)
Br(1)-Bi(1)-Br(4)^{iii}	97.80(2)	Bi(2)-Br(4)-Bi(1)^{iv}	96.14(2)

Symmetry codes: (*i*) *x*, -*y*+1/2, *z*+1/2; (*ii*) *x*, -*y*+1/2, *z*-1/2; (*iii*) *x*, *y*, *z*+1; (iv) *x*, *y*, *z*-1.

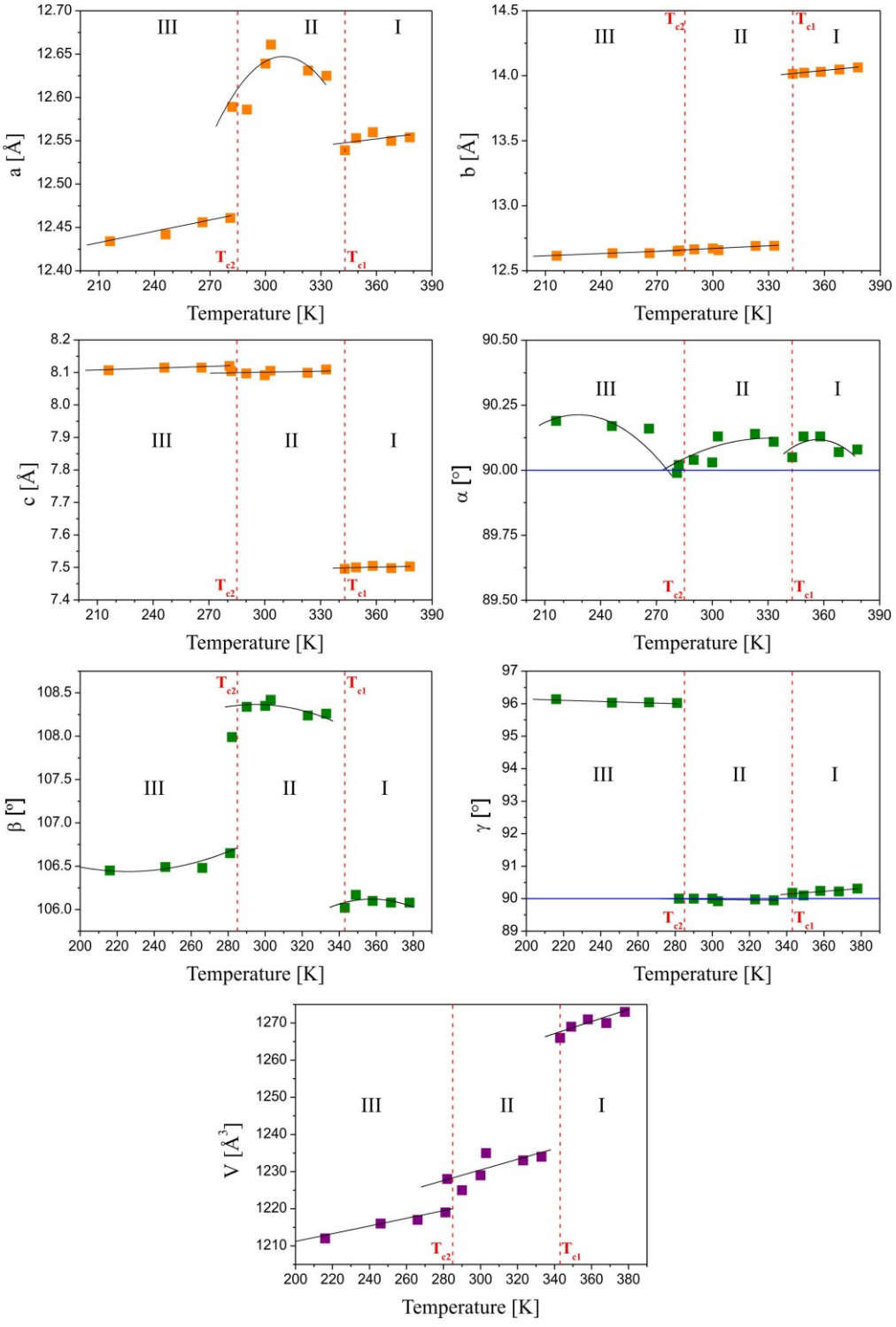

Figure S3. Variations of lattice parameters, presented in triclinic symmetry, of [*morph*]$BiBr_4$.

4 Vibrational characteristics of [*morph*]$BiBr_4$, [*morph*]$SbCl_4$ and [*morph*]$SbBr_4$

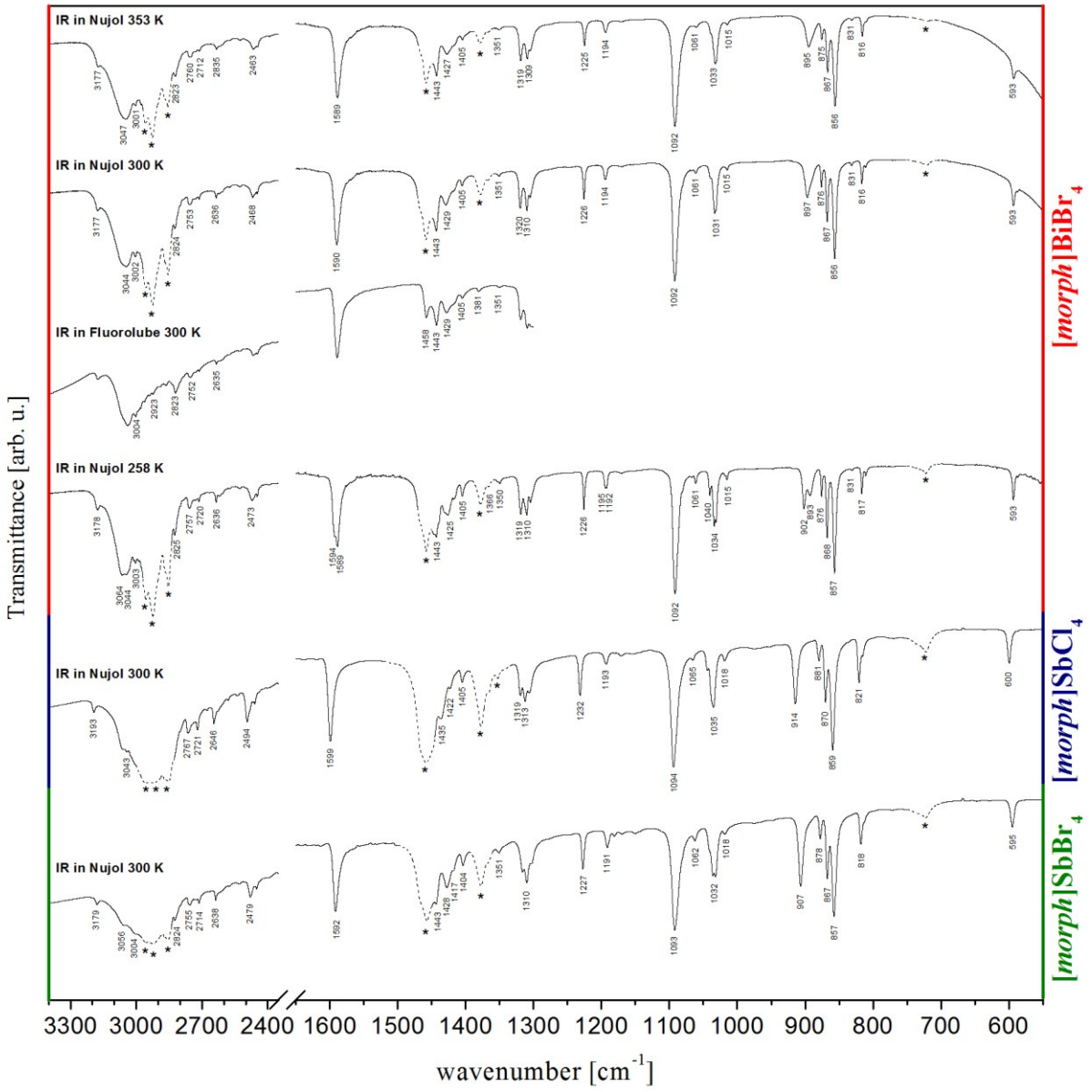

Figure S4. Infrared spectra of powdered [*morph*]$BiBr_4$ in Nujol (258, 300 and 373 K) and Fluorolube (300 K), and infrared spectra of [*morph*]$SbCl_4$ and [*morph*]$SbBr_4$. * - Nujol bands.

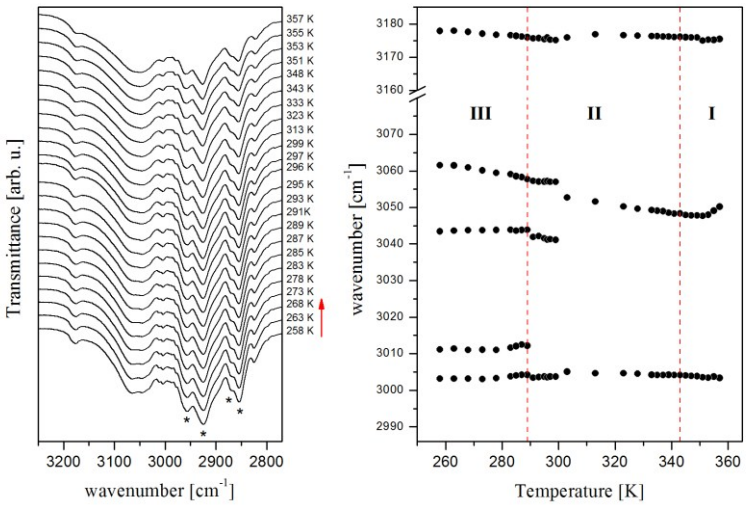

Figure S5. Evolution of IR spectra of [*morph*]$BiBr_4$ and temperature dependance of position of the selected bands arising from ν(NH_2) vibrations. * - Nujol bands.

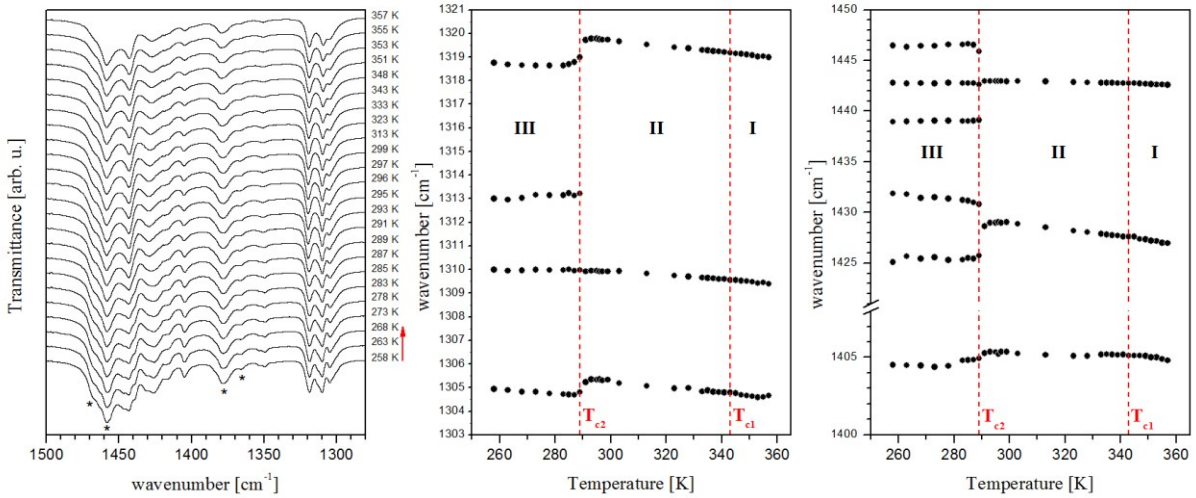

Figure S6. Evolution of IR spectra of [*morph*]$BiBr_4$ and temperature dependance of position of the selected bands arising from deformation vibrations of CH_2 groups (δ, ω) and wagging vibrations of NH_2 group. * - Nujol bands.

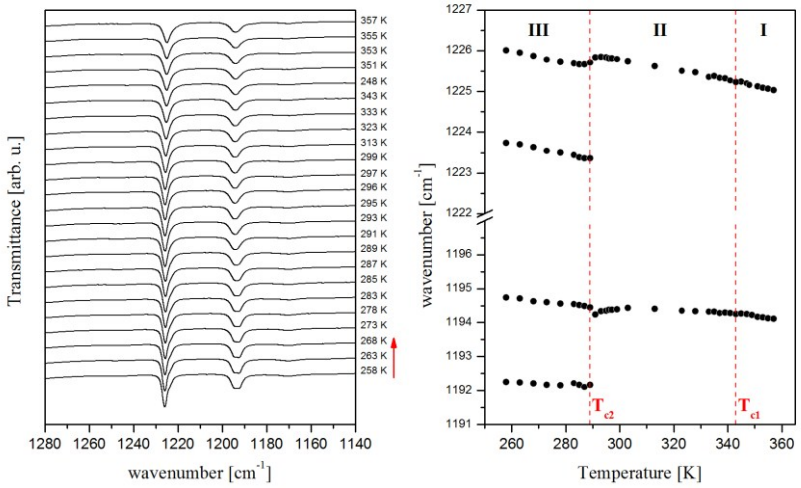

Figure S7. Evolution of IR spectra of [*morph*]$BiBr_4$ and temperature dependance of position of the selected bands arising from twisting vibrations of CH_2 groups and ν(C-N) vibrations.

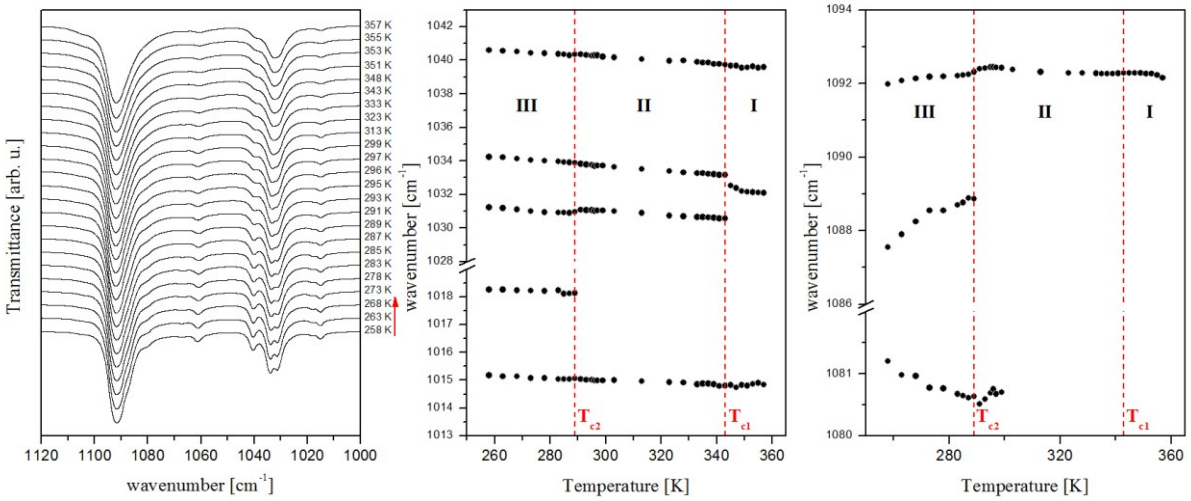

Figure S8. Evolution of IR spectra of [*morph*]$BiBr_4$ and temperature dependance of position of the selected bands arising from rocking vibrations of NH2 group and ν(C-N), ν(C-O) vibrations.

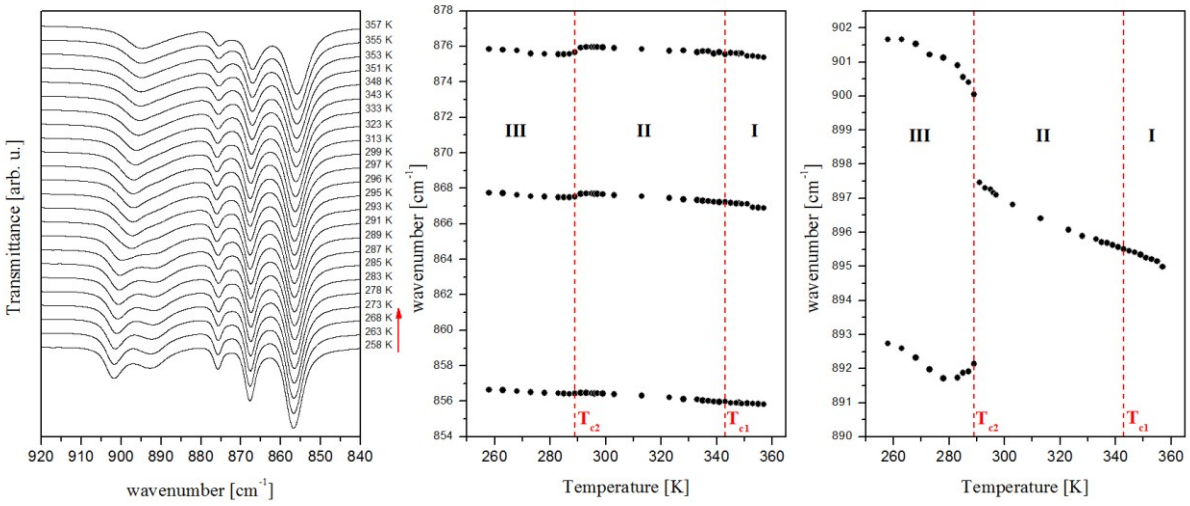

Figure S9. Evolution of IR spectra of [*morph*]$BiBr_4$ and temperature dependance of position of the selected bands arising from rocking vibrations of CH_2 groups and ν(C-C) vibrations.

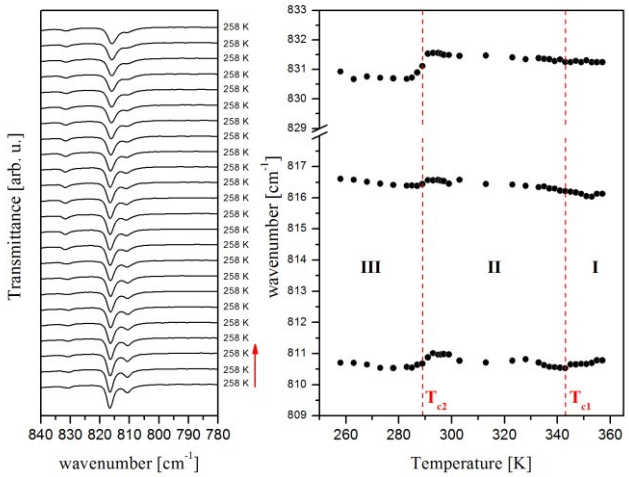

Figure S10. Evolution of IR spectra of [*morph*]$BiBr_4$ and temperature dependance of position of the selected bands arising from ν(C-O) vibrations.

Table S3. Position (cm^{-1}), relative intensities and tentative assignments of the bands observed in the IR spectra of [*morph*]$BiBr_4$ at 258, 300 and 373 K. The tantative assignments were based on a IR spectrum of morpholine [1] and similar heterocyclic compounds [2-5], as well as on experimental and theoretical data obtained for morpholinium tetrafluoroborate [6]. The assignments of the (NH_2) group were made taking into account results reported for protonated secondary amines [7].

ν_{IR} [cm^{-1}]			Tentative assignments
353 K	**300 K**	**258 K**	
3177(w)	3177(vw)	3178(w)	
3047(s)	3044(s)	3064(s)	
		3044(s)	$\nu(NH_2)$ or N-H…Br
		3011(m)	
3001(s)	3004*(m)	3003(s)	
	2990*(sh)		
	2980*(m)		
	2961*(m)		$\nu(CH_2)$
	2941*(w)		
	2923*(m)		

	2896*(w)		
	2867*(w)		
	2839*(sh)		
2823(w)	2823*(m)		
2760(vw)		2757(vw)	
2752(vw)	2752*(m)		
2730(vw)	2732*(w)	2730(vw)	
2712(vw)	2713*(w)	2720(vw)	
2635(vw)	2635*(w)	2636(vw)	
2617(vw)	2620*(vw)	2622(vw)	
		2614(vw)	
2605(vw)	2605*(vw)		combination bands
	2574*(vw)		
	2527*(vw)		
2466(vw)	2470*(w)	2473(vw)	
2447(vw)	2447*(w)	2448(vw)	
1589(s)	1590(s)	1594(m)	$\delta_{sciss}(NH_2)$
		1589(m)	
	1458*(s)		
		1446(sh)	$\delta(CH_2)$
1443(m)	1443*(s)	1443(m)	
		1439(sh)	
1427(w)	1429*(m)	1432(sh)	
1418(sh)		1425(w)	$\omega(NH_2)$
1415(sh)	1416*(sh)	1415(vw)	
1405(vw)	1405(vw)	1405(vw)	$\delta(CH_2)$
	1381*(w)		
1351(vw)	1351*(w)	1350(vw)	$\tau(NH_2)$
1319(w)	1320(w)	1319(w)	
		1313(sh)	$\omega(CH_2)$
1309(w)	1310(w)	1310(w)	
1305(sh)	1305(w)	1305(w)	
1225(w)	1226(w)	1226(w)	ν(C-N)
		1224(sh)	
1194(vw)	1194(vw)	1195(vw)	$\tau(CH_2)$
		1192(vw)	
1092(vs)	1092(vs)	1092(vs)	$\rho(NH_2)$
		1088(sh)	
1060(vw)	1061(vw)	1061(vw)	
1040(sh)	1040(w)	1041(w)	
1033(m)		1034(m)	ν(C-O) and ν(C-N)
1030(sh)	1031(sh)	1031(sh)	
1015(vw)	1015(vw)	1015(vw)	
		902(w)	$\rho(CH_2)$
895(w)	897(w)	893(w)	
875(w)	876(w)	876(w)	ν(C-C)
867(m)	868(m)	868(m)	
856(vs)	856(vs)	857(vs)	
831(vw)	831(vw)	831(vw)	
816(vw)	816(w)	817(w)	ν(C-O)
811(sh)	811(vw)	811(vw)	
593(w)	593(w)	593(w)	$\rho(CH_2)$
	588(vw)	587(vw)	

vs – very strong, v – strong, m – medium, w – weak, vw – very weak;

ν – stretching, δ_{sciss} – scissoring, ω – wagging, τ – twisting, ρ - rocking;
* obtained from the spectrum in Fluorolube

Table S4. Position (cm^{-1}), relative intensities and tentative assignments of the bands observed in the IR spectra of [*morph*]$SbCl_4$ and [*morph*]$SbBr_4$ at 300 K. For abreviations of symbols see footnote of Table S4.

[*morph*]$SbCl_4$	[*morph*]$SbBr_4$	Tentative assignments
ν_{IR} [cm^{-1}] 300 K	ν_{IR} [cm^{-1}] 300 K	
3193(vw)	3179(vw)	
3063(m)	3056(w)	
3043(m)		
3028(m)		$\nu(NH_2)$ or N-H…X
3010(sh)	3004(s)*	
2989(s)*	2982(s)*	
2968(s)*	2965(sh)*	
2937(sh)*	2934(sh)*	
2922(sh)*	2921(sh)*	
2898(m)*	2889(m)*	
2868(m)*	2865(m)*	
2845(m)*	2839(sh)*	
2831(s)*	2824(m)*	$\nu(CH_2)$
2794(sh)*	2799(sh)*	
	2782(sh)*	
2767(w)	2763(vw)	
	2755(vw)	
2721(w)	2727(vw)	
	2714(vw)	
2677(vw)		
2646(w)	2638(vw)	
2628(sh)		
	2619(sh)	
	2603(sh)	combination bands
2494(w)		
2480(sh)	2479(w)	
2468(vw)		
2458(vw)	2450(vw)	
1599(s)	1592(s)	$\delta_{sciss}(NH_2)$
1457(s)*	1457(s)*	
1452(s)*		$\delta(CH_2)$
1447(s)*	1443(s)*	
1435(m)*	1428(s)*	$\omega(NH_2)$
1422(m)*	1417(m)*	
1405(m)*	1404(m)*	$\delta(CH_2)$
1378(w)*	1378(w)*	
1353(w)*	1351(w)*	$\tau(NH_2)$
1319(w)	1317(w)	
1313(m)	1310(m)	$\omega(CH_2)$
1306(w)	1302(w)	
1232(w)	1227(w)	ν(C-N)
1193(vw)	1191(vw)	$\tau(CH_2)$
	1181(vw)	
	1169(vw)	
	1150(vw)	
1094(vs)	1093(s)	$\rho(NH_2)$
1065(vw)	1062(vw)	

1044(w) 1035(m) 1018(vw)	1036(m) 1032(m) 1018(vw)	ν(C-O) and ν(C-N)
914(m)	907(s)	$\rho(CH_2)$
881(vw) 870(m) 859(vs)	878(w) 867(s) 857(vs)	ν(C-C)
821(w) 815(vw)	818(w)	ν(C-O)
600(w)	595(w)	$\rho(CH_2)$

5 Optical observations of [*morph*]$BiBr_4$

Observations of a ferroelastic domain structure were performed under OLYMPUS BX53 polarizing microscope.

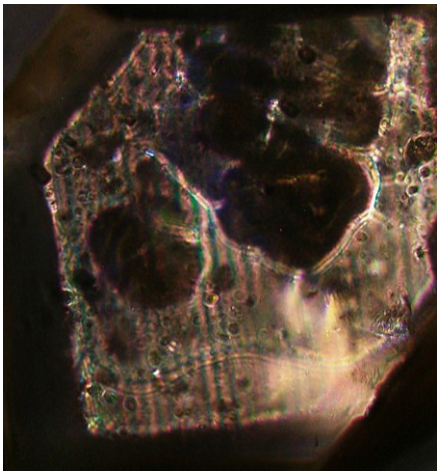

Figure S11. The traces of ferroelastic domain structure of [*morph*]$BiBr_4$.

6 Dielectric properties of [*morph*]$SbCl_4$

The frequency dependence of complex electric permittivity $\varepsilon^* = \varepsilon' - i\varepsilon''$ of [*morph*]$SbCl_4$ was measured between 130 and 300 K with an Agilent 4980A Precision LCR Meter in the frequency range 100 Hz to 2 MHz along crystallographic *a* direction. The dimensions of the samples used in these measurements were approximately 4 × 4 × 1 mm^3. Silver graphite electrodes were painted onto opposite large faces. The overall error in electric permittivity measurements was less than 5%.

The dielectric response at low temperature was well described by the Cole–Cole relation:

$$\varepsilon^*(\omega) = \varepsilon_\infty + \frac{\varepsilon_o - \varepsilon_\infty}{1 + (i\omega\tau)^{1-\alpha}} \quad (1)$$

The experimental Cole–Cole plots at several temperatures were fitted to Eq. (1) and the fitting parameters ε_0, ε_∞, α and τ were determined. In the systems characterized by weak dipole–

dipole interactions we can assume that the macroscopic relaxation time is equivalent to a microscopic one, thus the energy barrier E_a can be estimated from the Arrhenius relation for the macroscopic relaxation time:

$$\tau = C \exp\left(\frac{E_a}{kT}\right) \tag{2}$$

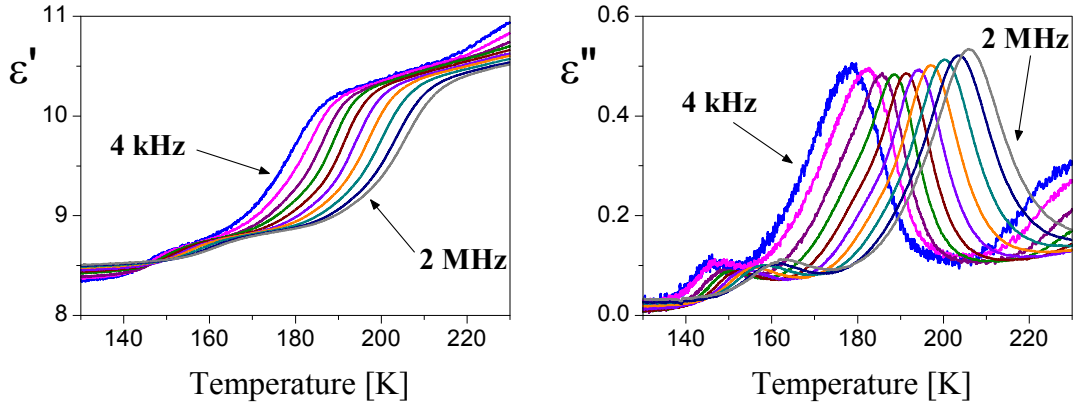

Figure S12. Temperature dependence of the real and imaginary parts of of the complex electric permittivity obtained on cooling cycle.

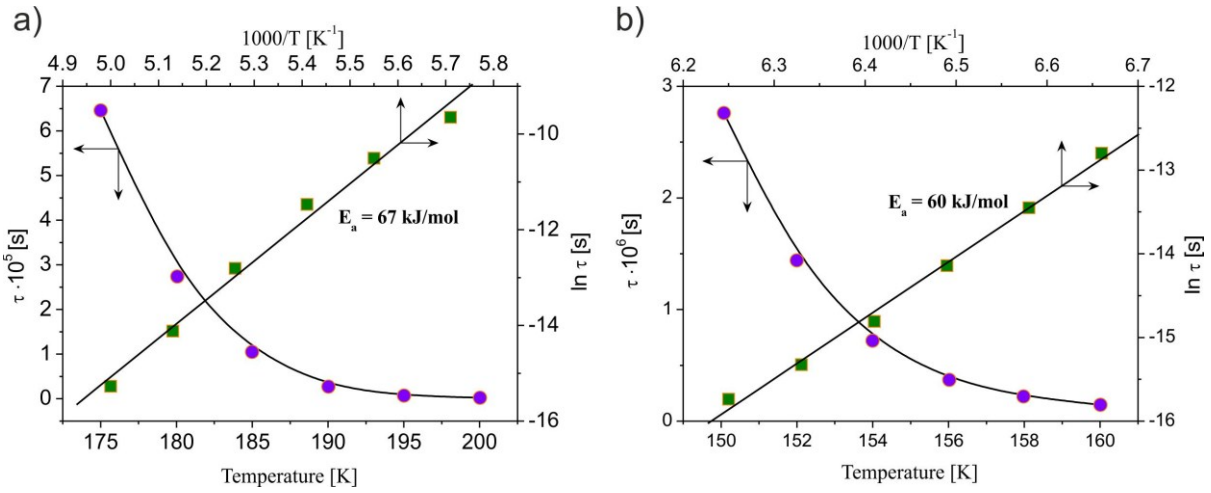

Figure S13. Plots of relaxation times τ versus temperature and lnτ versus reciprocal temperature for the high temperature (a) and low temperature relaxator (b).

References

[1] D. Vedal, O. H. Ellestad, P. Klaboe, *Spectrochim. Acta,* 1976, **32A**, 877.
[2] O. H. Ellestad, P. Klaboe, *Spectrochim. Acta*, 1973, **29A**, 1247.
[3] D. Vedal, O. H. Ellestad, P. Klaboe, *Spectrochim. Acta*, 1975, **31A**, 339.
[4] D. Vedal, O. H. Ellestad, P. Klaboe, *Spectrochim. Acta*, 1975, **31A**, 355.
[5] O. H. Ellestad, P. Klaboe, *Spectrochim. Acta*, 1971, **27A**, 1025.
[6] M. Owczarek, R. Jakubas, G. Bator, A. Pawlukojć, J. Baran, J. Przesławski, W. Medycki, *Chem. Phys.*, 2011, **381**, 11.
[7] D. Cook, Can. *J. Chem.,* 1964, **42**, 2292.

Comment to the [*morph*]$BiBr_4$ structure determination at 210 K.

The phase transition from the phase II (belonging to the monoclinic symmetry) to the phase III (triclinic) is connected with the twinnig of the sample. In our experiment in the phase III dominated two types of domains. The domain I, which permitted indexing of 57% reflections, and the domain II to which 35% reflections belonged. The matrix of the transformation among these two domains is as follows: -1 0 0 -1 -0.215 0 0 1. The structure was found for the collection of reflections of the domain I. Final refinement of the crystal structure was carried out using the collection of reflections of both types of domains. The figures S14 and S15 show the visualizations of Ewald sphere for the both types of reflections.

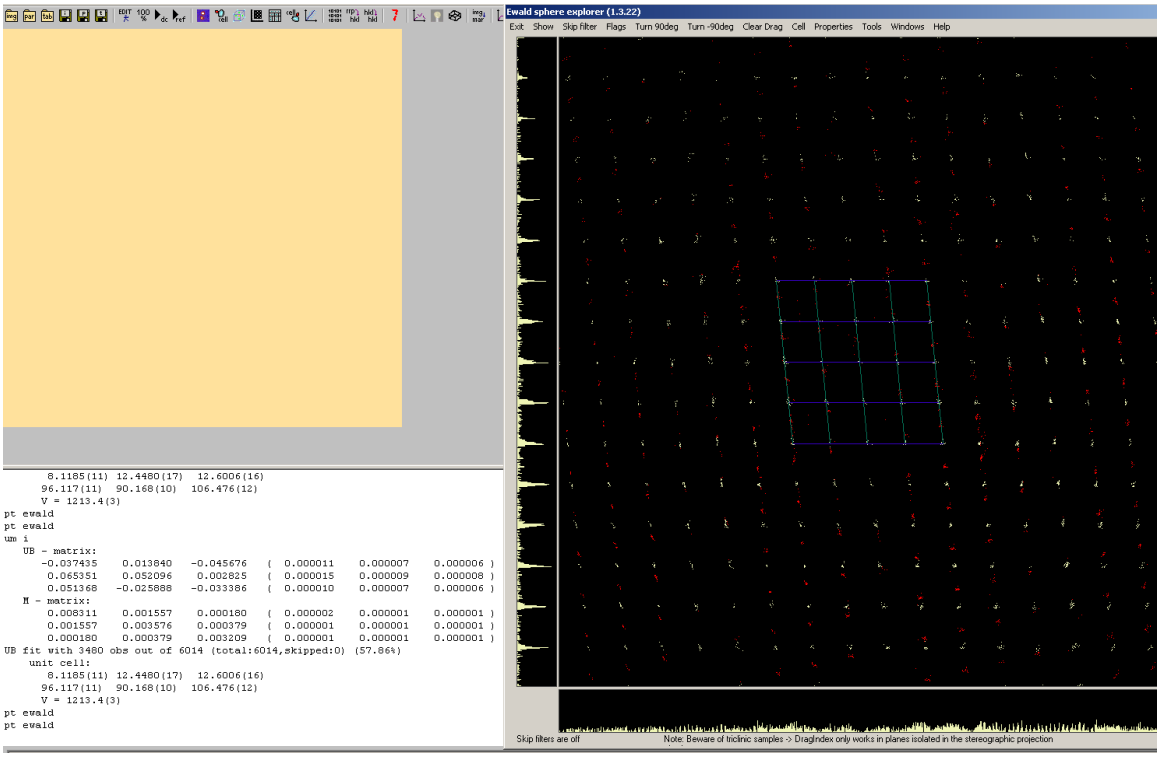

Figure S14. Domain I.

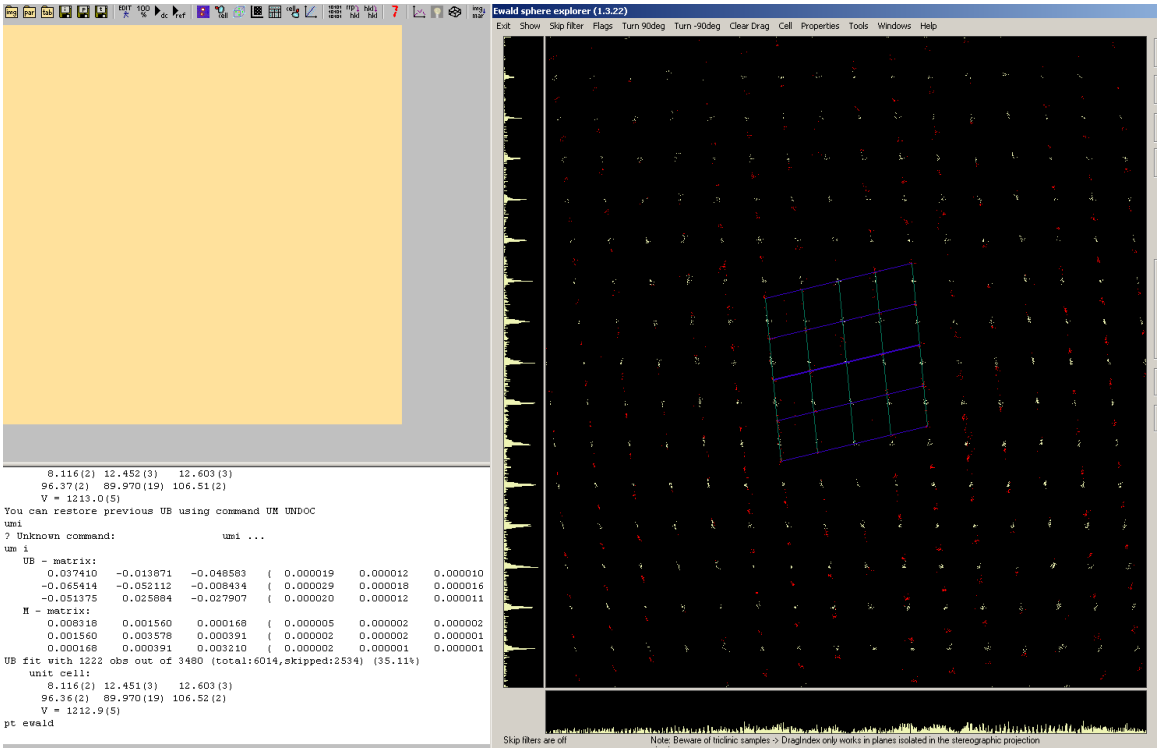

Figure S15. Domain II.